


J. J. Derksen  · A. E. Komrakova

Multiscale simulations of sliding droplets

Received: 15 February 2018 / Revised: 15 June 2018 / Published online: 30 October 2018
© The Author(s) 2018

Abstract We study—through numerical simulations—a droplet sliding over a solid substrate as a result of a simple shear flow. We use a free-energy lattice Boltzmann (LB) scheme and compare its results with those of molecular dynamics (MD) simulations. According to the MD, at sufficiently low Reynolds and capillary numbers, the dimensionless sliding speed is a unique function of the equilibrium contact angle. Reproducing the MD results with LB simulations requires the use of a non-equilibrium boundary condition at the substrate and tuning a free parameter in the boundary condition.

1 Introduction

Multiphase flow in porous media has a number of technological applications. A prominent one is water flooding as a method for (enhanced) oil recovery [1]. Water (sea water, brine) is injected in rock formations containing oil in an attempt to sweep out the hydrocarbons. It is not easy to predict the success of such an oil recovery operation given the complexity of the system [2]: the geometrical complexity of the pore structure, the physicochemical interaction between the substrates (pore walls) and the fluids, and the interfacial effects between (saline) water and hydrocarbon mixtures (oil). Modeling the pore-scale processes taking place during water flooding operations through numerical simulations potentially is a means of enhancing the understanding and thus predictability of the operations.

An important element of such simulation efforts is an accurate representation of moving three-phase contact lines [3]. These are the locations where substrate, oil, and water are in contact. Given the displacement objectives of flooding operations, we expect these contact lines to move, i.e., slide over the substrate. This sliding implies slip of fluids over solid surfaces, something that needs very careful attention when modeling the flow and interfacial dynamics based on continuum assumptions [4]. It has, in fact, been argued that contact line slip is essentially a molecular phenomenon, i.e., can only be described properly by viewing the fluids and solid as constituted of (discrete) molecules [5].

In a previous paper [6], we have investigated contact line motion from a molecular perspective (i.e., by using molecular dynamics, MD) for a relatively simple situation: a sessile drop of Fluid 1, immersed in Fluid 2 with the two immiscible fluids undergoing simple shear. The two fluids had the same density and viscosity; what separates them is their mutual surface tension. A key result of this study is a relationship between the dimensionless sliding speed of the drop of Fluid 1 and the static contact angle of the drop on the substrate.

J. J. Derksen (✉)
School of Engineering, University of Aberdeen, Aberdeen, UK
E-mail: jderksen@abdn.ac.uk

A. E. Komrakova
Mechanical Engineering, University of Alberta, Edmonton, Canada

Since molecular simulations can only handle nanoscopic systems, we want to generalize the results for sliding speeds obtained at the molecular level [6] to continuum models. The present paper focuses on options of how to deal with this generalization. We have performed continuum simulations by means of the lattice Boltzmann method of the same systems as studied with MD [6]. The key choices that need to be made in the continuum simulations relate to the boundary conditions at the substrate. In making these choices, we were guided by the results from the MD simulations as obtained in [6].

The aim of this paper thus is to assess the role of the substrate boundary conditions when performing continuum simulations of drops sliding over solid surfaces where results of molecular simulations are used as a benchmark. The continuum simulations are based on a free-energy, multiphase lattice Boltzmann scheme [7] with a multiple relaxation time collision operator [8]. This is a diffuse interface method with an order parameter that distinguishes between the two liquid phases. Boundary conditions at the substrate are formulated in terms of the order parameter and its gradient normal to the substrate. We will be comparing results obtained with equilibrium and non-equilibrium boundary conditions.

The paper is organized in the following manner: We will start by defining the flow system in terms of a set of dimensionless numbers, and by summarizing the earlier work on representing this system through MD simulations. We then describe the free-energy lattice Boltzmann formulation and discuss the options for substrate boundary conditions. Results section comprises of droplet sliding speeds and droplet deformations, their sensitivity for the boundary conditions, and a comparison between continuum and MD results. In the final section, we summarize and reiterate conclusions.

2 Flow configuration and molecular dynamics results

We consider the volume between two parallel solid plates. On the bottom plate, a semispherical drop of radius R_0 consisting of Fluid 1 is placed; the rest of the volume between the plates contains Fluid 2. Both fluids are Newtonian with density ρ and kinematic viscosity ν . The surface tension between the two fluids is denoted as γ . First the system is equilibrated so that a drop of Fluid 1 develops a certain equilibrium contact angle θ . Once equilibrated, the two plates start moving relative to one another thereby creating a steady shearing motion with average shear rate G between the plates. This whole process is schematically depicted in Fig. 1, which also defines the coordinate system that will be used throughout this paper.

As the dimensionless parameters characterizing the sheared droplet process, we choose a capillary number $Ca \equiv \rho\nu GR_0/\gamma$, a Reynolds number $Re \equiv GR_0^2/\nu$, the equilibrium contact angle θ , and the aspect ratio R_0/H with H the distance between the plates (see Fig. 1). We will be having near-creeping flow ($Re \ll 1$) and expect limited effects of the finite width (H) of the flow systems so that the main dependencies will be on Ca and θ .

The system as described above was the subject of MD simulations in [6] with $0.04 \leq Ca \leq 0.64$ and $65^\circ \leq \theta \leq 111^\circ$. The fluids were Lennard–Jones (LJ) liquids with spherical molecules of mass m and diameter σ . The LJ interaction potential between molecule i and j that have center-to-center distance r_{ij} was expressed as $u_{ij}^{LJ}(r_{ij}) = 4\epsilon \left[(\sigma/r_{ij})^{12} - d_{\alpha\beta} (\sigma/r_{ij})^6 \right]$. The simulations were performed under isothermal conditions with $k_B T/\epsilon = 0.68$ (T is temperature, k_B the Boltzmann constant) and density such that $\rho\sigma^3 = 0.84$. The factor $d_{\alpha\beta}$ is a non-standard feature [6,9]. For molecules of the same fluid $d_{\alpha\alpha} = 1$; by making $d_{12} < 1$, we create surface tension between the two fluids; by tuning the way the two fluids interact with the solid material the plates are made of, we establish an equilibrium contact angle. For instance, if Fluid 1 and 2 interact in the same way with the solid, a 90° angle is established. The calibrations required to relate the set of $d_{\alpha\beta}$'s to

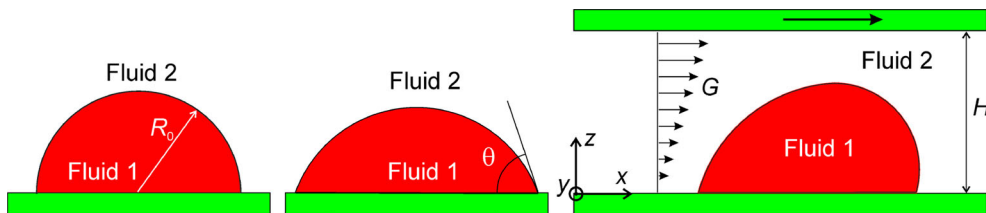


Fig. 1 Schematic of the drop formation and shearing process. From left to right: immerse Fluid 1 in Fluid 2 as a hemisphere on a substrate; let the system equilibrate and generate a shear flow with shear rate G . Results will be presented in a frame of reference such that the lower substrate has zero velocity

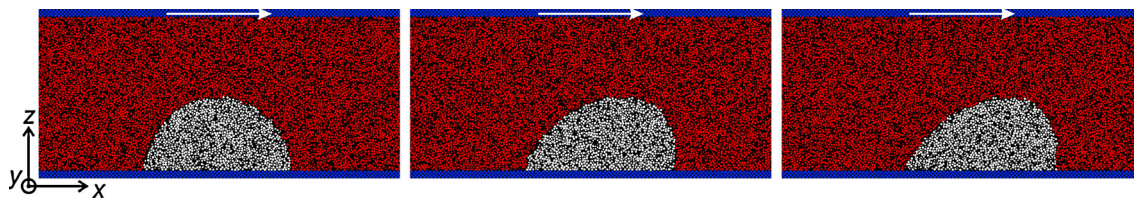


Fig. 2 Sample MD result. Snapshots of cross sections through the three-dimensional domain. White: Fluid 1; red: Fluid 2; blue: solid. $Ca = 0.040$, $\theta = 90^\circ$. Time increasing from left to right: $tG = 0.002$, 0.353 , 0.704 with $t = 0$ the moment shear is started (color figure online)

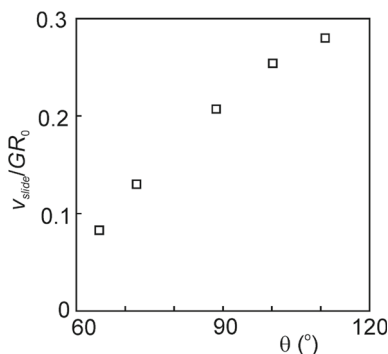


Fig. 3 Droplet sliding speed relative to shear rate times initial drop radius as a function of the static contact angle. Molecular dynamics results [6]

surface tension and contact angle have been described in detail in [6]. For all LJ interactions, a cut-off distance of 2.5σ was applied.

A typical result of an MD simulation is shown in Fig. 2. Note that in this figure—as well as for the rest of the results presented—the reference frame is such that the lower plate is standing still and the upper plate is moving to the right. All simulations have been performed such that in a static frame of reference both plates are moving with the same speed but in opposite direction. In the series of snapshots, we see the drop deforming as a result of the shearing motion of the plates and also see relative motion between the footprint of the drop and the lower wall. The speed of this sliding motion—also given the applications of oil recovery—is considered the most relevant outcome of the MD simulations as it relates to mobilizing Fluid 1. For $Ca \leq 0.32$, the sliding speed was to a very good approximation proportional to the capillary number [6]. This allowed us to define a dimensionless sliding speed v_{slide}/GR_0 that—at least in the linear regime—is only a function of the equilibrium contact angle θ . Figure 3 shows this relationship. The dimensionless sliding speed increases with increasing contact angle. This is because at increasing contact angle the drop protrudes further into the shear flow field, and because Fluid 1 (the drop) has a smaller area of contact with the substrate.

3 Continuum simulations—free-energy lattice Boltzmann method

The scenario of placing a drop on a solid substrate, equilibration, and then shearing it as described above has been followed through in lattice Boltzmann (LB) simulations. By matching Ca , θ , Re , and R_0/H with the MD simulations, it is ensured that a direct comparison between MD and LB results can be made.

The two-dimensional simulation procedure due to Pooley et al. [10] has been extended to three dimensions. It is a free-energy multiphase LB scheme. In 3D, it uses a 19 speed model (D3Q19) with lattice velocities \mathbf{e}_i $i = 0, \dots, 18$ (1 zero velocity; 6 velocities in the Cartesian coordinate directions, $|\mathbf{e}_i| = 1$; 12 in diagonal directions $|\mathbf{e}_i| = \sqrt{2}$). Space is discretized by a grid of uniform cubic cells. As often is done in an LB context, we will be working in lattice units (lu) with the lattice spacing the unit of length, and the time step the unit of time. Two distribution functions are applied: $f_i(\mathbf{x}, t)$ for flow dynamics (so that fluid density and momentum are described by $\rho = \sum_{i=0}^{18} f_i$ and $\rho\mathbf{u} = \sum_{i=0}^{18} f_i\mathbf{e}_i$, respectively), and $g_i(\mathbf{x}, t)$ for the order parameter $\phi = \sum_{i=0}^{18} g_i$. The order parameter distinguishes between the two fluids: $\phi = 1$ in Fluid 1; $\phi = -1$ in Fluid 2; $-1 < \phi < 1$ in the interface between the two fluids. It satisfies the following transport equation:

$$\frac{\partial \phi}{\partial t} + \nabla \cdot (\phi \mathbf{u}) = M \nabla^2 \mu \quad (1)$$

with M the mobility and $\mu = a(-\phi + \phi^3) - \kappa \nabla^2 \phi$ the chemical potential [7]. Surface tension and interface thickness (symbol ξ) are determined by the parameters a and κ : $\gamma = \frac{2}{3} \sqrt{2\kappa a}$ and $\xi = \sqrt{2\kappa/a}$.

Integration of Eq. (1) is performed through a standard LB-BGK scheme where the mobility M relates to the relaxation time τ_g in the BGK collision operator [7]: $M = \Gamma (\tau_g - \frac{1}{2})$. The coefficient of mobility Γ is a tunable parameter which is part of the equilibrium distribution g_i^{eq} [10]. As concluded in [10], accuracy is greatly enhanced by applying a multiple relaxation time (MRT) scheme for updating the hydrodynamic distribution function $f_i(\mathbf{x}, t)$. In three dimensions, the collision operations as used in MRT have been detailed in [8].

As flow boundary conditions, the half-way bounce-back rule was applied for achieving no-slip at the solid walls; periodic conditions apply in the x and y direction. The boundary condition for the order parameter ϕ at the lower solid surface—which is the surface the drop is attached to—determines the contact angle. For static, i.e., non-shear, situations two different equilibrium boundary conditions have been tested; the first [10] is

$$\sqrt{\frac{2\kappa}{a}} \frac{\partial \phi}{\partial n} \Big|_{z=0} = 2 \operatorname{sgn} \left(\theta - \frac{\pi}{2} \right) \sqrt{\cos \left(\frac{\alpha}{3} \right) \left[1 - \cos \left(\frac{\alpha}{3} \right) \right]} \quad (2)$$

with $\alpha = \arccos(\sin^2 \theta)$. Equation (2) is an exact result obtained through minimizing a free-energy expression that includes a surface term [10]. The second boundary condition [11] reads

$$-\sqrt{\frac{2\kappa}{a}} \frac{\partial \phi}{\partial n} \Big|_{z=0} = (\phi^2 - 1) \cos \theta \quad (3)$$

It represents an approximate energy minimization neglecting some higher-order terms in the free-energy function as detailed in [12]. As we will see, both conditions successfully create a drop with the desired equilibrium contact angle θ . At the top surface, $\partial \phi / \partial n = 0$ is imposed; in x - and y -direction, boundary conditions are periodic.

In the shear simulations, we have—next to the two equilibrium boundary conditions (2) and (3)—also tested a non-equilibrium boundary condition at the bottom surface as proposed in [13]. It is a phenomenological extension with an unsteady term of Eq. (3):

$$D_w^* \frac{\partial \phi}{\partial t} = \kappa \frac{\partial \phi}{\partial n} + \frac{\sqrt{2}}{2} \sqrt{a\kappa} (\phi^2 - 1) \cos \theta \quad (4)$$

with D_w^* a dimensional parameter (SI units N s/m) that in [13] is interpreted in terms of a hopping process of fluid molecules at the surface of the substrate. It has been non-dimensionalized as $D_w \equiv D_w^*/(\rho \nu R_0)$. It is clear that in steady state, Eq. (4) reduces to Eq. (3).

The spatial resolution of the LB simulations is such that R_0 corresponds to 30 lattice units (lu). Komrakova et al. [14] have performed a benchmark study based on a liquid droplet deforming under shear to find a set of LB parameters that shows stable and accurate results for a wide range of capillary numbers. In line with that study, we set the liquid density to $\rho = 1$, the kinematic viscosity to $\nu = 1/6$ (note that Fluid 1 and Fluid 2 have the same density and viscosity), the relaxation time $\tau_g = 1$, and the coefficient of mobility $\Gamma = 2$. The interface thickness relative to the drop size is known as the Cahn number, it was set to $Ch \equiv \xi/R_0 = 0.0337$ so that $\xi = 1.01$. This has been achieved by $a = 2.275 \times 10^{-3}$ (lu) and $\kappa = 1.164 \times 10^{-3}$ (lu). The surface tension then is $\gamma = 0.00153$ (lu). The size of the computational domain is $n_x \cdot n_y \cdot n_z = 150 \cdot 101 \cdot 64$ so that $R_0/H = 30/64 \approx 0.469$.

Variations in Ca were achieved by varying the shear rate G which—given the fixed size of the computational domain in z -direction—has been done by varying the shearing velocity of the plates. At the default value of $Ca = 0.16$, the upper plate has a velocity of $+0.00157$ (lu), the lower plate of -0.00157 (lu), i.e., it takes about 20,000 time steps for one of the plates to move over a distance R_0 . At this value of Ca , $Re = 0.26$. Variations in the equilibrium contact angle θ are imposed through the boundary condition on the lower plate (via Eqs. (2), (3), or (4)).

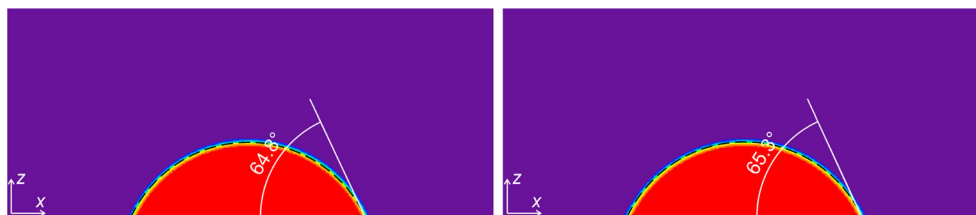


Fig. 4 Lattice Boltzmann simulation results: equilibrated droplets with application of Eqs. (2) (right panel) and (3) (left panel) as boundary conditions at $z = 0$ with $\theta = 65^\circ$. The dashed curve is a circle that best fits the curve with order parameter $\phi = 0$. The “measured” angles have been derived from the fitted circle sections

4 Results

Cross sections through equilibrated drops are shown in Fig. 4. It can be seen that both equilibrium boundary conditions (Eqs. (2), (3)) are well able to recover accurately the contact angle that was given as input parameter to the boundary conditions. In results presented from now on, the default equilibrium boundary condition will be the one due to [11], i.e., Eq. (3).

After drops were equilibrated, the shearing motion was imposed, still applying the equilibrium boundary condition. In Fig. 5, we show for three static (i.e., equilibrium) contact angles and $Ca = 0.160$ the onset of the shearing process that results in drop deformation and a sliding motion relative to the lower substrate. Figure 6 shows the displacement of the drops relative to the lower substrate as a function of time. Shortly after the onset of the shearing motion ($t = 0$), the displacement gets linear with time and the drops are thus sliding with a constant speed. We confirmed that simulations with half the shear rate as applied in Fig. 6—that thus are at $Ca = 0.080$ —show half the sliding speed. As for the MD simulations, the LB simulations thus are in a linear regime.

Figure 7 summarizes the data on dimensionless sliding speeds as obtained through LB simulations with equilibrium boundary conditions (Eqs. (2), (3)); for reference, the data obtained with MD have been included in the figure. The trend is the same as in the MD simulations (shown in Fig. 3): an increase in dimensionless sliding speed with equilibrium contact angle. For the larger contact angles ($\theta > 90^\circ$), the agreement between LB and MD results is good; for the smaller contact angles, the LB simulations are significantly overpredicting the dimensionless sliding speeds.

A reason for this overprediction could be the application of an equilibrium boundary condition in an essentially non-equilibrium (sheared) system. The equilibrium boundary condition manifests itself in Fig. 5. Careful inspection of the three-phase contact points in the cross sections shown in Fig. 5 teaches that closely above the substrate the interface is forced to the equilibrium contact angle by the boundary condition; a dynamic receding and advancing contact angle different from the equilibrium angle seemingly cannot be accommodated well by the equilibrium boundary condition.

It is therefore natural to test the non-equilibrium boundary condition that is available in the form of Eq. (4). There is, however, no theory for the coefficient D_w^* in the unsteady term in Eq. (4) so that it is not possible to objectively select its value. It was first established that applying Eq. 4 has impact on the sliding speed and that in the limit of $D_w^* \rightarrow 0$ the sliding speed with Eq. (3)—which can be interpreted as the steady-state version of Eq. (4)—was recovered; see Fig. 8 where $\theta = 65^\circ$ and $Ca = 0.160$ has been taken as the sample situation. In line with what was done in [13], we then use D_w^* as a fitting parameter, i.e., we try to find a value for D_w^* such that the dimensionless sliding speed v_{slide}/GR_0 is approximately the same as in the MD simulation for a given equilibrium contact angle. For $\theta = 65^\circ$, this is achieved when $D_w \equiv D_w^*/(\rho\nu R_0) \approx 0.171$. The resulting drop deformations are shown in Fig. 9. Close to the three-phase contact line, the shape of the interface between Fluid 1 and Fluid 2 is different, more smooth, from what is observed in Fig. 5 (left column).

If the fitting procedure is applied for the other contact angles as well, the results in Fig. 10 are obtained. For the two largest contact angles investigated ($\theta = 100^\circ$ and 111°), $D_w = 0$ gives the best fit with the dimensionless sliding speeds as determined by MD. For the smaller contact angles, D_w decreases monotonically with increasing contact angle. This is in contrast to [13] where non-monotonic behavior with contact angle was observed when studying a droplet spreading process.

For the LB simulations that now exhibit a dimensionless droplet sliding speed comparable to the speed observed in MD simulations (i.e., the data points in Fig. 10), the deformation of the resulting drop has been compared to the deformation as observed in MD simulations at the same capillary number ($Ca = 0.16$). As a

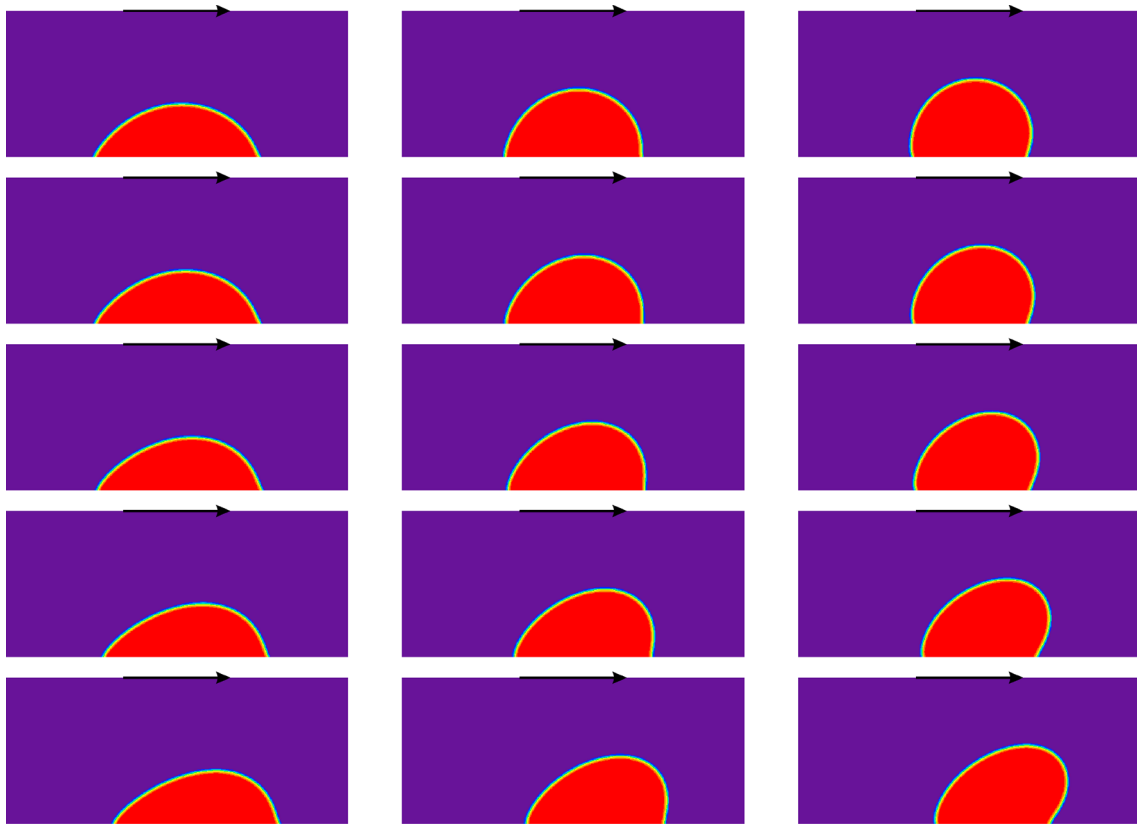


Fig. 5 Drop deforming and sliding with $Ca = 0.16$ and (from left to right) $\theta = 65^\circ$, 90° , 111° . Equilibrium boundary condition (according to Eq. (3)). Time (after starting shear) increases from top to bottom: $Gt = 0.0982$, 0.196 , 0.392 , 0.786 , 1.57 , respectively. In the frame of reference of this figure, the lower wall has zero velocity

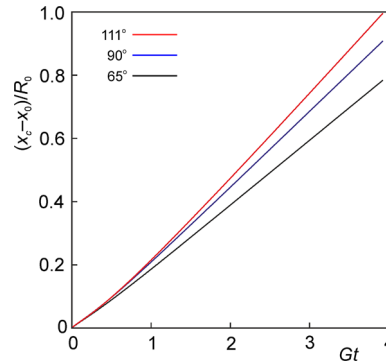


Fig. 6 Displacement of the center of the footprint of the drop x_c on the lower wall relative to its initial location x_0 as a function of time for three equilibrium contact angles. Use of equilibrium boundary condition (Eq. (3))

metric for drop deformation, the dynamic receding and advancing contact angles have been determined through fitting a circular arc through part of the interface in the same way as done in the MD simulations [6]. The results in Fig. 11 show significant differences between MD and LB results with the advancing angles generally significantly larger in LB simulations. From the right panels of Fig. 11, it is clear that a circular arc—as used in the fitting process—might not be an accurate way to represent the interface, specifically for the advancing angle, leading to a biased contact angle estimate which explains part of the differences observed.

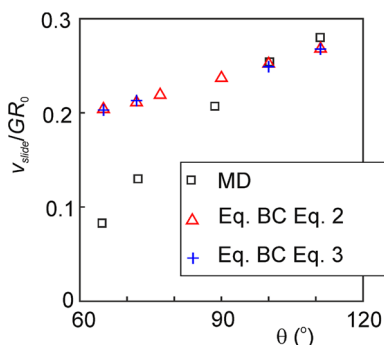


Fig. 7 Dimensionless droplet sliding speed as a function of the static contact angle. Lattice Boltzmann simulations with equilibrium boundary conditions (Eqs. (2), (3) as indicated) compared to MD results

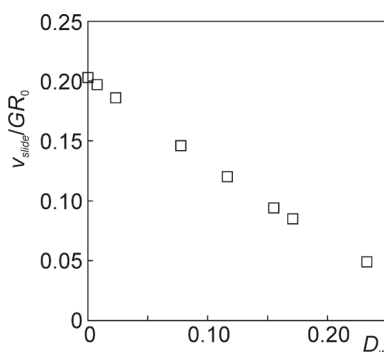


Fig. 8 Dimensionless sliding speed versus $D_w \equiv D_w^*/(\rho\nu R_0)$ (with D_w^* the coefficient of the unsteady term in the non-equilibrium boundary condition Eq. (4)); $Ca = 0.16$, $\theta = 65^\circ$. The $D_w = 0$ data point is the result of applying Eq. (3)

5 Summary and conclusions

We numerically studied the sliding of liquid drops immersed in another liquid over a substrate as a result of a simple shear flow. Such problems have relevance for multiphase flow in porous media as, e.g., encountered in oil recovery operations. Since the systems involve a moving three-phase contact line, continuum simulations require special attention to the boundary conditions at the substrate. In our lattice Boltzmann procedure, based on a free-energy approach and with a multiple relaxation time collision operator, equilibrium as well as non-equilibrium conditions were tested. Benchmark data from molecular dynamics simulations [6] were used to assess the predictions by the LB method.

Droplet sliding speeds were generally overpredicted by the LB simulations if equilibrium boundary conditions were used. Also the interface shape close to the substrate shows slightly anomalous behavior in such cases. The non-equilibrium boundary conditions we tested are not fully predictive, i.e., we do not a priori know the relative strength of the unsteady term it contains. If we use the latter as a fitting parameter, and if we allow this fitting parameter to be a function of the equilibrium contact angle, we were able to match the dimensionless sliding speeds as observed in molecular dynamics simulations.

Further work thus needs to focus on a better understanding of the physics behind the unsteady term in the non-equilibrium boundary condition and analyze why it needs to depend on the contact angle to match the molecular dynamics data. Involving the deformation of the sliding drop—including estimating dynamic contact angles—might be beneficial in such an analysis. At present, we do not observe a good agreement of dynamic contact angles of drops sliding at the same dimensionless speed in molecular dynamics and lattice Boltzmann simulations.

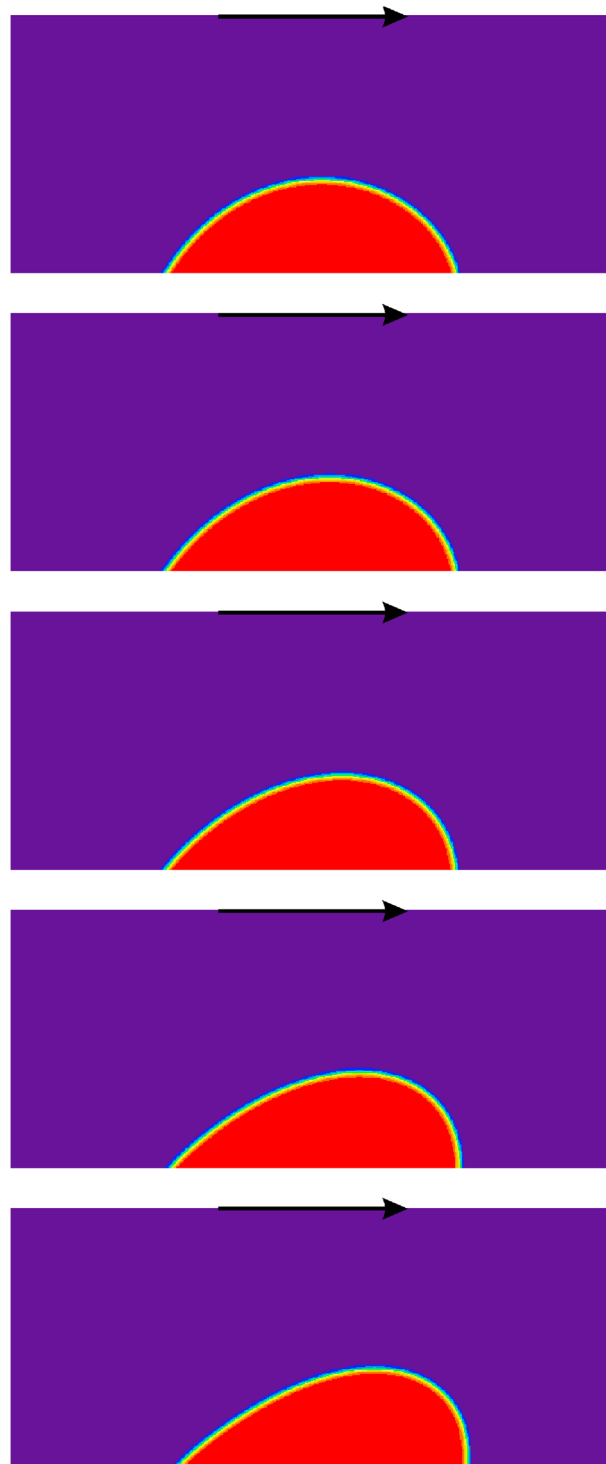


Fig. 9 Drop deforming and sliding with $Ca = 0.16$ and $\theta = 65^\circ$. Non-equilibrium boundary condition with $D_w = 0.171$. Time (after starting shear) increases from top to bottom: $Gt = 0.0982, 0.196, 0.392, 0.786, 1.57$, respectively. In the frame of reference of this figure, the lower wall has zero velocity

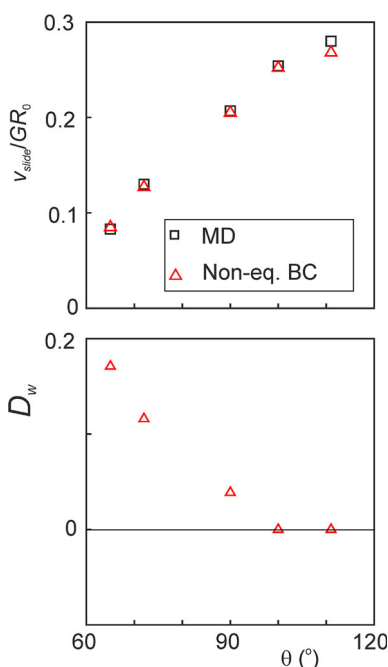


Fig. 10 Bottom: fitted coefficient D_w as a function of equilibrium contact angle; top: the resulting dimensionless droplet sliding speed as obtained with the non-equilibrium boundary condition compared to the MD results

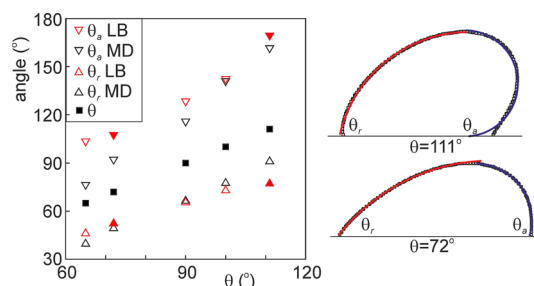


Fig. 11 Receding and advancing contact angles θ_r and θ_a as a function of the static contact angle θ , comparison between MD results [6], and LB results for $Ca = 0.16$. The contact angles have been measured by fitting circles to the interface on the receding and advancing side of the drop, respectively, as illustrated on the right (the filled red symbols relate to the right panels). The filled black symbols show—for reference—the static contact angle

Open Access This article is distributed under the terms of the Creative Commons Attribution 4.0 International License (<http://creativecommons.org/licenses/by/4.0/>), which permits unrestricted use, distribution, and reproduction in any medium, provided you give appropriate credit to the original author(s) and the source, provide a link to the Creative Commons license, and indicate if changes were made.

References

- Sheng, J.J.: Critical review of low-salinity waterflooding. *J. Pet. Sci. Technol.* **120**, 216–224 (2014)
- Desmond, J.L., Juhl, K., Hassenkam, T., Stipp, S.L.S., Walsh, T.R., Rodger, P.M.: Organic-silica interactions in saline: elucidating the structural influence of calcium in low-salinity enhanced oil recovery. *Sci. Rep.* **7**, 10944 (2017)
- Cox, R.G.: The dynamics of the spreading of liquids on a solid surface. Part 1. Viscous flow. *J. Fluid Mech.* **168**, 169–194 (1986)
- Jacqmin, D.: Contact-line dynamics of a diffuse fluid interface. *J. Fluid Mech.* **402**, 57–88 (2000)
- Blake, T.D.: The physics of moving wetting lines. *J. Colloid Interface Sci.* **299**, 1–13 (2006)
- Derksen, J.J.: Droplets sliding over shearing surfaces studied by molecular dynamics. *AIChE J.* **61**, 4020–4027 (2015)
- Swift, M.R., Orlandini, E., Osborn, W.R., Yeomans, J.M.: Lattice Boltzmann simulations of liquid–gas and binary fluid systems. *Phys. Rev. E* **54**, 5041–5052 (1996)
- Yu, H., Luo, L.S., Girimaji, S.S.: LES of turbulent square jet flow using an MRT lattice-Boltzmann model. *Comput. Fluids* **35**, 957–965 (2006)

9. Koplik, J., Banavar, J.R.: Molecular structure of the coalescence of liquid interfaces. *Science* **257**, 1664–1666 (1992)
10. Pooley, C.M., Kusumaatmaja, H., Yeomans, J.M.: Contact line dynamics in binary lattice Boltzmann simulations. *Phys. Rev. E* **78**, 056709-1-9 (2008)
11. Liu, H., Valocchi, A.J., Zhang, Y., Kang, Q.: Lattice Boltzmann phase-field modeling of thermocapillary flows in a confined microchannel. *J. Comput. Phys.* **256**, 334–356 (2014)
12. Lee, T., Liu, L.: Lattice Boltzmann simulations of micron-scale drop impact on dry surfaces. *J. Comput. Phys.* **229**, 8045–8063 (2010)
13. Carlson, A., Do-Quang, M., Amberg, G.: Dissipation in rapid dynamic wetting. *J. Fluid Mech.* **682**, 213–240 (2011)
14. Komrakova, A.E., Shardt, O., Eskin, D., Derksen, J.J.: Lattice Boltzmann simulations of drop deformation and breakup in shear flow. *Int. J. Multiph. Flow* **59**, 24–43 (2014)

Publisher's Note Springer Nature remains neutral with regard to jurisdictional claims in published maps and institutional affiliations.